

**Supporting Information for:**

**Large Area Mosaic Films of Graphene-Titania: Self-Assembly at the Liquid-air interface and Photoresponsive Behavior**

**Timothy N. Lambert,<sup>\*a</sup> Carlos A. Chavez,<sup>a</sup> Nelson S. Bell,<sup>b</sup> Cody M. Washburn,<sup>c</sup> David R. Wheeler<sup>d</sup> and Michael T. Brumbach<sup>e</sup>**

*Sandia National Laboratories, Albuquerque, New Mexico, 87185*

*Department of:*

<sup>a</sup> Materials, Devices and Energy Technologies

<sup>b</sup> Electronic & Nanostructured Materials

<sup>c</sup> Organic Materials

<sup>d</sup> Biosensors and Nanomaterials

<sup>e</sup> Materials Characterization,

Sandia National Laboratories, Albuquerque, New Mexico 87185

\*Author to whom correspondences should be sent: Department of Materials, Devices and Energy Technologies P.O. Box 5800, MS-0734, Sandia National Laboratories, Albuquerque, New Mexico, 87185; Ph. (505) 284-6967, Fx. (505) 844-7786, E-mail: [tnlambe@sandia.gov](mailto:tnlambe@sandia.gov).

## Experimental Details.

### Synthesis

In a typical synthesis, 100 mg of 0.04 M TiO<sub>2</sub>-GO<sup>1</sup> was dispersed with sonication (60 min) in 100 mL of deionized water in a 125 mL Erlenmeyer flask. The sample was exposed to a 900 W UV lamp (20 cm away) for 3-5 h while stirring. The solution turned from a brown color to a black color, with some precipitate formation, during the exposure. The reaction was transferred to centrifuge tubes and spun at 3500 rpm for 10 min. The black solution (supernatant) was placed aside. The precipitate was washed with water (50 mL) and MeOH (30 mL), and these washes were added to the original supernatant. The combined solutions (sol-TiO<sub>2</sub>-RGO) were allowed to sit undisturbed loosely covered where upon SA-TiO<sub>2</sub>-RGO films formed at the air-liquid interface over several days.

### Characterization

*Scanning Electron Microscopy (SEM).* SA-TiO<sub>2</sub>-RGO films were deposited on a silicon wafer and imaged using a Zeiss Supra 55VP field emitter gun scanning electron microscope (FEGSEM). A Noran EDS detector and Noran System Six software were used for the acquisition of the EDS spectra. EDS Data was plotted using Kaleidagraph™ software.

*X-ray photoelectron spectroscopy.* X-ray photoelectron spectroscopy (XPS) was performed with a Kratos Axis Ultra DLD with monochromatic Al K $\alpha$  (1486.6 eV) source at 225 W, and an analyzer pass energy of 20 eV as previously described.<sup>2</sup> The analyzed spot size was 300 x 700 microns and base pressures were less than 5 x 10<sup>-9</sup> Torr. Charge neutralization was used for all samples. Energy normalization was performed, by setting the first primary component of the C 1s spectrum at 284.5 eV. Data were analyzed using CasaXPS software. Peaks were fit using a Shirley background and a Gaussian/Lorentzian line shape. Peak positions and FWHM for C 1s values were allowed to vary within a limited range, since identical fitting constraints could not be used to fit all spectra.

*Raman Spectroscopy.* Raman spectra were recorded using a Thermo Scientific Smart Raman DXR instrument with a DRX 633 nm laser with a high-resolution gradient from 150 cm<sup>-1</sup> to 2100 cm<sup>-1</sup>. Resulting data was analyzed using the Thermo Scientific Software and re-plotted for presentation purposes using Kaleidograph software.

*X-ray Diffraction (XRD).* SA-TiO<sub>2</sub>-RGO films were collected onto a zero background holder purchased from The Gem Dugout, State College, PA 16803 and allowed to dry. Samples were scanned at a rate of 0.02°/2 s in the 2θ range of 5–80° on a Bruker D8 Advance diffractometer in Bragg-Brentano geometry with Cu K $\alpha$  radiation and a diffracted beam graphite monochromator.

*Transmission Electron Microscopy (TEM).* A SA-TiO<sub>2</sub>-RGO film was placed directly onto a holey carbon type-A, 300 mesh, copper TEM grid purchased from Ted Pella, Inc., Redding, CA 96049 and allowed to dry. Films were studied using a JEOL 2010 high resolution transmission electron microscope (HRTEM), operating at 200 kV accelerating voltage.

*Dynamic Light Scattering (DLS) and Zeta ( $\zeta$ ) Potential Measurements.* DLS and zeta potential measurements were performed using a Zetasizer Nano ZS instrument from Malvern. This instrument utilizes laser Doppler velocimetry with phase analysis light scattering to calculate the particle size distribution and the zeta potential with a red laser (633 nm).  $\zeta$ -potential characterization was performed in background electrolyte of 10<sup>-3</sup> M KNO<sub>3</sub>, and titrated with HNO<sub>3</sub> and KOH for pH adjustment.

*Interdigitated Electrode (IDE) Fabrication.* A standard lift off technique of titanium and gold was patterned on quartz substrates. The 100 mm quartz wafers were primed and coated using AZ 4110 photoresist, which was spin coated on at 4000 rpm for 30 seconds. A 90 °C for 30 seconds pre-bake produces a 1.1 μm thick layer. The use of a Karl Suss contact aligner with a 365 nm notch filter was used to expose the photo-resist, and the pattern was opened using a standard development recipe. An adhesion layer using 20 nm of Ti was deposited followed by the deposition of 300 nm of Au<sup>0</sup> in a Temescal evaporator. A pitch of 10 micron establishes the 400 μm longer finger for a total edge length of 2 mm. The outside die dimensions are 4 mm by 8 mm and contain four identical channels that are 1 mm of interdigitated electrode.

*RGO Testing Conditions.* The SA-TiO<sub>2</sub>-RGO thin film was placed orthogonal to the metallic trace that is approximately 1 mm in width. Each of the interdigitated channels is connected to form a signal and ground pin-out connection to a Kiethley 6517 electrometer with LabView interface for data acquisition. The channels were wire bonded at the chip level and connected via a circuit board for ease of handling and to minimize noise during photo-current measurements. A West Bond wedge tip bonder was utilized, with gold wire and a stage temperature of 100 °C for optimal bond conditions. Bonding after or prior to SA-TiO<sub>2</sub>-RGO film deposition gave similar test results.

*Uv excitation of thin films.* A Horiba Fluorolog Spectrometer was used for UV generation, which can go down to 250 nm wavelength using a xenon lamp for exposure. The lamp intensity is in a range from 25 to 30 mJ/cm<sup>2</sup> and varies slightly with warm up time on the power supply and wavelength of interest. The xenon lamp has a decrease in intensity as a function of deep ultra violet wavelengths due to the excitation energy from xenon gas in these wavelengths. A 30 min wait was used before exposure to the sample. The circuit board containing the sample (SA-TiO<sub>2</sub>-RGO/IDE) was placed in the line of site to the lamp to maximize photo-current during exposure. First, incremental wavelengths at 50 nm intervals were used to determine the best excitation

wavelength for exposure. This experiment started at 600 nm and finished at 250 nm, with a change in wavelength occurring at 10 min increments. The photo-current had the most significant change at 350 nm and this roughly coincides with the energy band gap of titanium dioxide. A noticeable shift at 250 nm, corresponding to the decay of intensity due to the xenon source, was also observed. Photocurrent measurements were then conducted with an excitation wavelength of 350 nm. All measurements were done using the fluorimeter enclosure to minimize laboratory lighting as a possible source of noise and error in the data collection. Initial change in resistance measurements were performed using a Black-Ray UV lamp that delivered long-wave (365 nm) ultra-violet light with  $\sim 21.7 \text{ mJ/cm}^2$  at a 5 cm working distance.

*Colloidal Properties and Modeling.* The method for calculating the surface parameters in the van Oss-Chaudry-Good model (VOCG).<sup>3,4</sup> The development of the treatment is as follows. The Young equation relates the contact angle to the force balance at the drop edge for the liquid surface tension ( $\gamma_L$ ), the solid surface energy ( $\gamma_S$ ) and the interfacial energy between the solid and liquid ( $\gamma_{SL}$ ).

$$\gamma_L \cos \theta = \gamma_S - \gamma_{SL} \quad (1)$$

Dupré, in turn, determined an equation to describe the work of adhesion:

$$\Delta G_{SL} = \gamma_{SL} - \gamma_S - \gamma_L \quad (2)$$

The Young-Dupré Equation results from combining these relationships.

$$-\Delta G_{SL} = \gamma_L(1 + \cos \theta) \quad (3)$$

The VOCG approach determines an expression for the free energy of interaction between the solid and liquid ( $\Delta G_{SL}$ ), based on the  $\gamma^{LW}$ ,  $\gamma^+$  and  $\gamma^-$  properties of the solid and liquid materials. The liquid parameters are tabulated as a scale based on the assumption that the electron donating and accepting properties of water are equal, and the Lifshitz-Van der Waals component of the surface tension is related to the Hamaker constant of the material. ( $l_0$  is approximated as 1.57 Å.)

$$A_{ii} = 24 \pi l_{0PVP}^2 \gamma_i^{LW} \quad (4)$$

The solid surface requires an expression for the interaction between the components of the surface energies of the liquid and solid phases (in equilibrium with the atmosphere). That expression is as follows.

$$\gamma_{SL} = \left( \sqrt{\gamma_S^{LW}} - \sqrt{\gamma_L^{LW}} \right)^2 + 2 \left( \sqrt{\gamma_S^+ \gamma_S^-} + \sqrt{\gamma_L^+ \gamma_L^-} - \sqrt{\gamma_S^+ \gamma_L^-} - \sqrt{\gamma_S^- \gamma_L^+} \right) \quad (5)$$

In this method, the contact angle is measured for each film using three liquids. One liquid is purely dispersive, and the other two have been characterized for their acid and base components. The following equation is used with each fluid and contact angle ( $\theta$ ) to determine the surface parameters of each film.

$$(1 + \cos \theta) \gamma_L = 2(\sqrt{\gamma_S^{LW} \gamma_L^{LW}} + \sqrt{\gamma_S^+ \gamma_L^-} + \sqrt{\gamma_S^- \gamma_L^+}) \quad (6)$$

The apolar liquid has no acid (+) or base (-) components, and therefore should interact only by van der Waals interactions. Using a liquid with known values of  $\gamma_L$ ,  $\gamma_L^{LW}$ ,  $\gamma_L^+$  and  $\gamma_L^-$  for contact angle measurements leaves three unknowns in the equation— $\gamma_S^{LW}$ ,  $\gamma_S^+$  and  $\gamma_S^-$ . It is therefore necessary to make contact angle measurements using three different liquids, all with known values of  $\gamma_L$ ,  $\gamma_L^{LW}$ ,  $\gamma_L^+$  and  $\gamma_L^-$ . The calculate values of  $\gamma_S^{LW}$ ,  $\gamma_S^+$  and  $\gamma_S^-$  can then be used with equation 6 to determine  $\gamma_S$ :

$$\gamma_S = \gamma_S^{LW} + 2\sqrt{\gamma_S^+ \gamma_S^-} \quad (7)$$

The obtained values of  $\gamma_S$  can then be used with the known values of  $\gamma_L$  in equation 1 to determine  $\gamma_{SL}$ .<sup>3</sup> Solving for the apolar probe liquid (diiodomethane), gives a value for the dispersive component of the RGO films of 34.2 mJ/m<sup>2</sup>. This value is substituted into the values for the remaining two equations. This results in values of  $\gamma_S^+ = 0.897$  mJ/m<sup>2</sup> and  $\gamma_S^- = 2.619$  mJ/m<sup>2</sup>. This material is a weak electron donor. This likely relates to the  $\pi$  bonding character of the reduced material. The overall surface energy properties of the material suggest that it has low polarity components overall, and the use of polar solvents for dispersion should not be promoted. The zeta potential measured earlier should be the relevant dispersion mechanism in water, and adding MeOH to the water may lead to poorer dispersion of this material.

The surface energy parameters determined using the VOCG model can be used to determine the free energy of wetting of the surface (1) within the fluid (3) using the following relationship.

$$\Delta G_{131} = -2\left(\sqrt{\gamma_1^D} - \sqrt{\gamma_3^D}\right)^2 - 4\left(\sqrt{\gamma_1^+ \gamma_1^-} + \sqrt{\gamma_3^+ \gamma_3^-} - \sqrt{\gamma_1^+ \gamma_3^-} - \sqrt{\gamma_3^+ \gamma_1^-}\right) \quad (8)$$

Using these parameters, an energy of wetting for the films can be calculated using equation 8. This gives a value of  $\Delta G_{131} = -59.09$  mJ/m<sup>2</sup>.

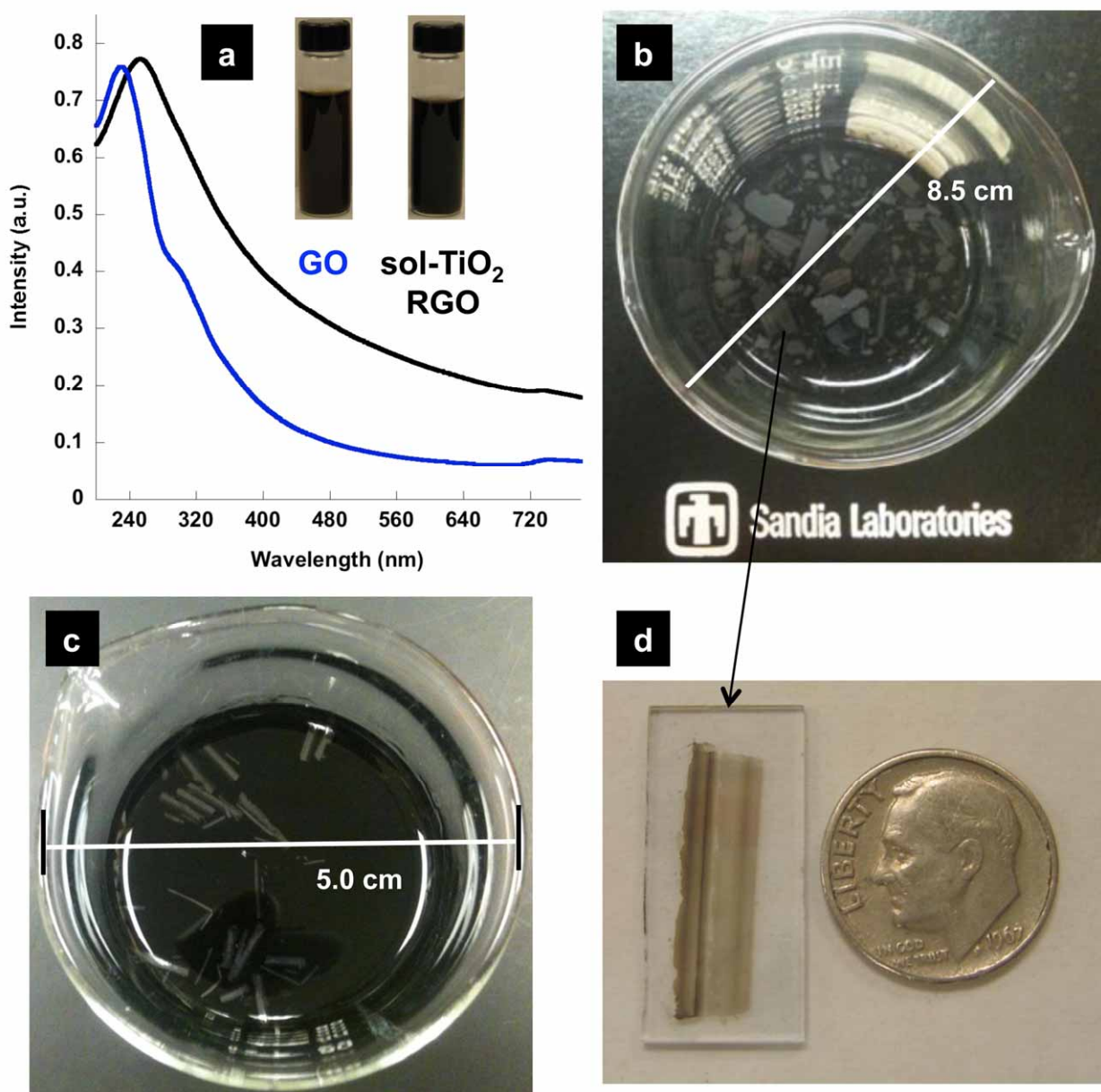


**Figure S1.** a) UV-vis spectra and picture of aqueous GO and sol-TiO<sub>2</sub>-RGO; b) and c) SA-TiO<sub>2</sub>-RGO thin films prepared from the UV-photo-reduction of sol-TiO<sub>2</sub>-RGO. Two morphologies were observed: high aspect rectangles and square-like shaped films; d) A SA-TiO<sub>2</sub>-RGO film deposited onto ITO. The striping indicates varying thickness and non-uniformity across the film in the side-to-side (short axis dimension) direction. This is a result of films “annealing” at the liquid-air interface.

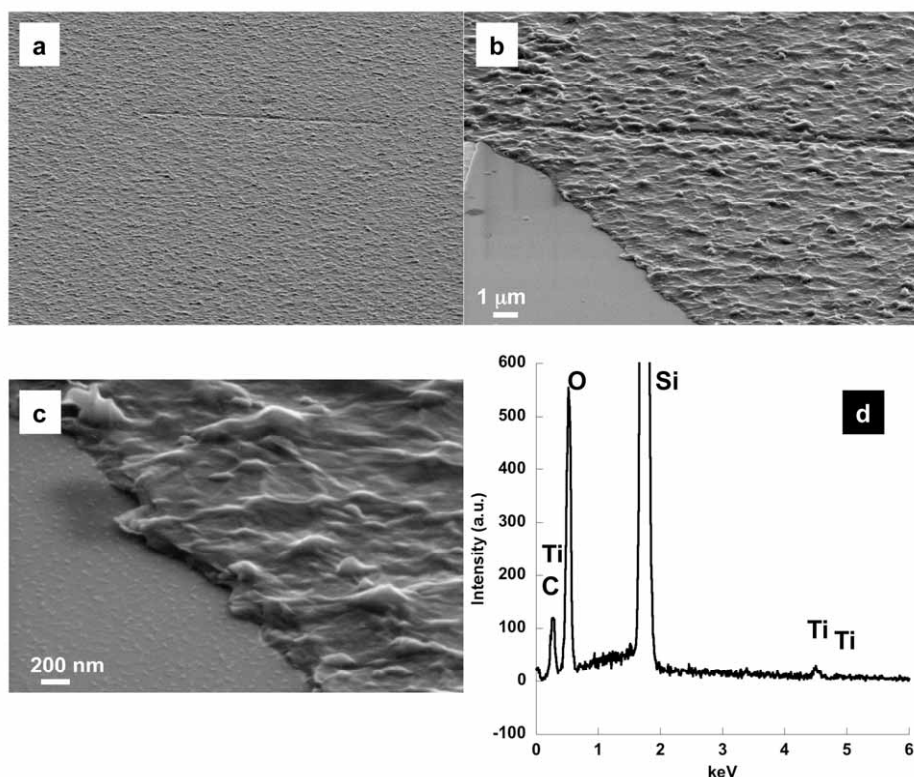


**Figure S2.** a)-c) SEM micrographs and d) EDS of a SA-TiO<sub>2</sub>-RGO thin film deposited onto a SiO<sub>x</sub>/Si wafer.

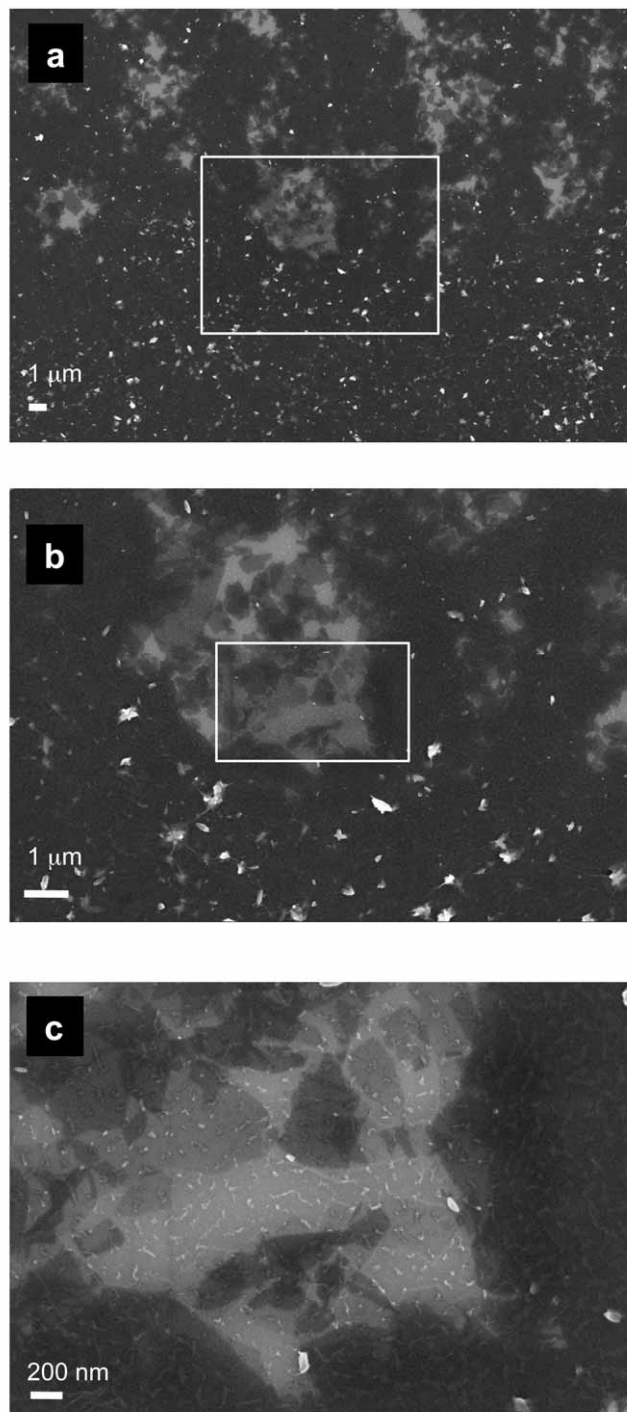


**Figure S3.** a)-c) SEM micrographs of a SA-TiO<sub>2</sub>-RGO thin film (high aspect ratio rectangle) collected shortly after formation. Images show the film is comprised of a mosaic assembly of smaller TiO<sub>2</sub>-RGO sheets.

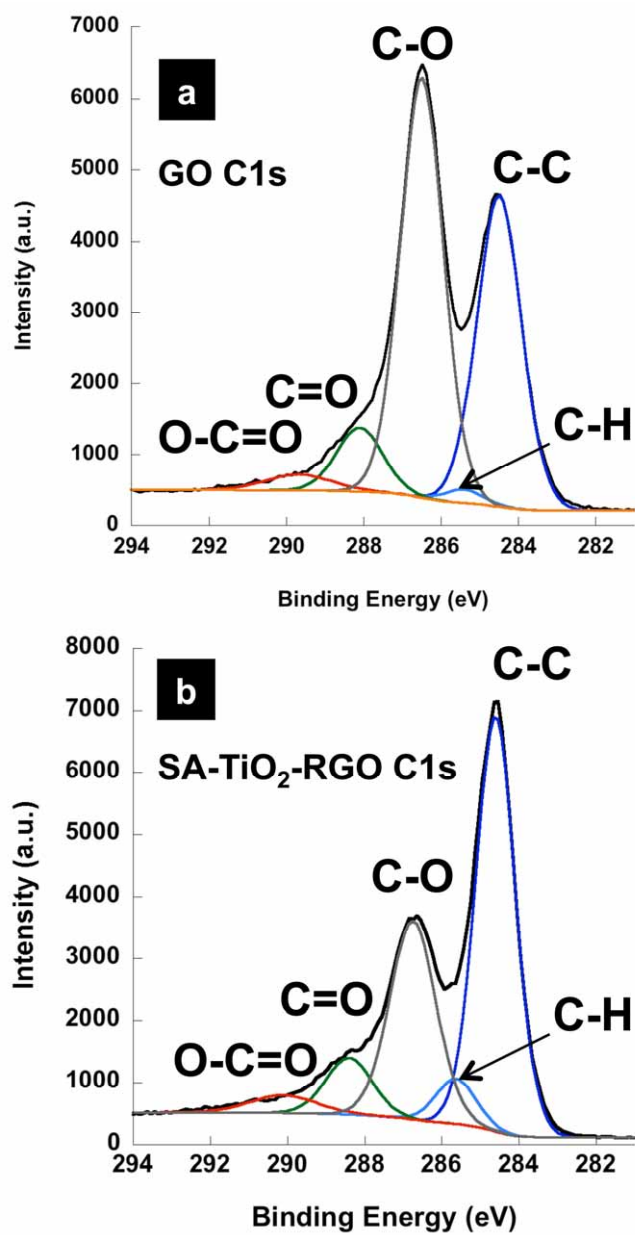


**Figure S4.** XPS spectra of a) GO and ) SA-TiO<sub>2</sub>-RGO thin film.

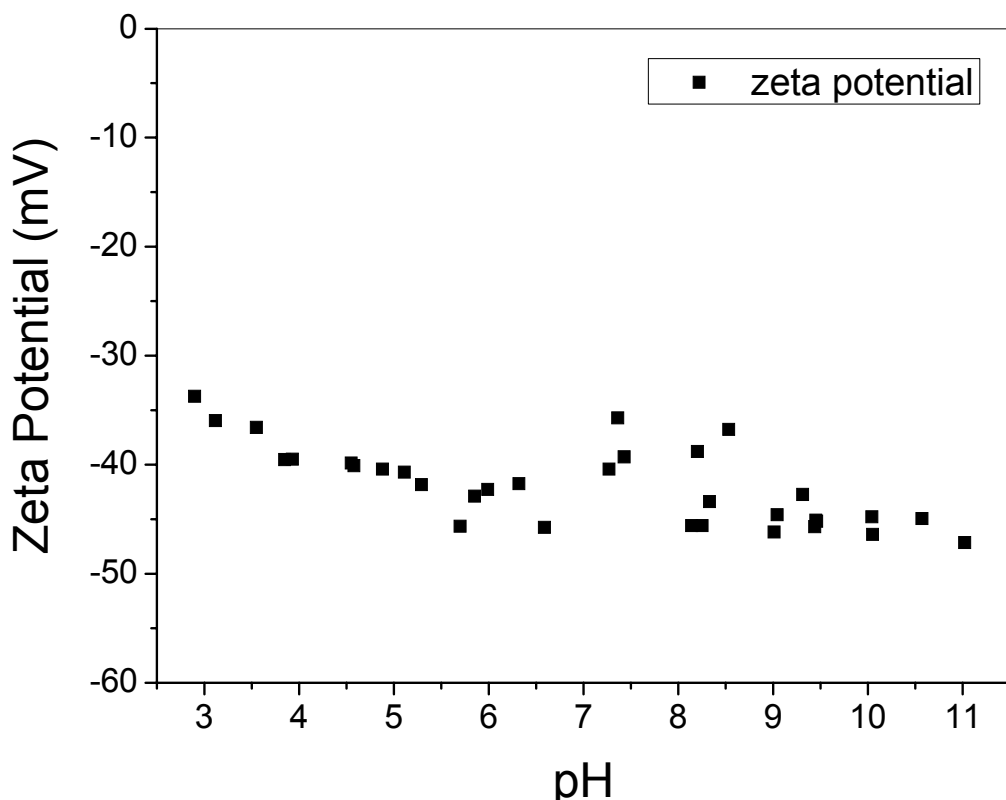


**Figure S5.** a) Zeta ( $\zeta$ ) potential measurements on sol-TiO<sub>2</sub>-RGO as a function of pH in 10<sup>-3</sup> M KNO<sub>3</sub> electrolyte. Measurements were taken using a Malvern Instruments Zetasizer NS under dilute particle conditions (i.e. optically clear solutions).

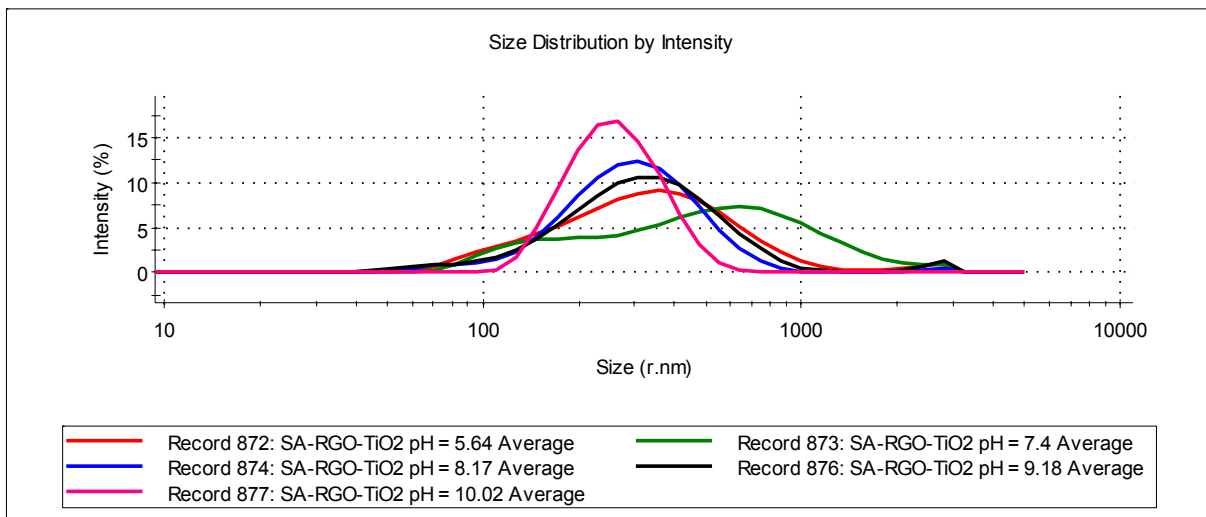


**Figure S6.** Size determination of sol-TiO<sub>2</sub>-RGO as determined using dynamic light scattering.

The particle size distributions measured by light scattering show a trend of decreasing peak position with increasing pH, reflecting the increase in measured  $\zeta$ -potential, with one exception found at pH 7.4. This value of the solution pH gave the most variation in the value of  $\zeta$ -potential as well, and will require a more in depth study to determine the reason for this behavior. A hypothesis under consideration relates to the surface charging of the titania nanoparticles; TiO<sub>2</sub> can have an isoelectric point between 3 to 9 depending on the preparation method. Potentially, the titania nanoparticles can be positively charged under acidic conditions, but are electrostatically bound within/on the negative GO nanosheets. As pH rises, the TiO<sub>2</sub> can become neutral or negatively charged leading to increased dispersion. The anomalous increase in particle size could result from the partial de-binding of nanosheets into looser aggregates, followed by complete dispersion for the particles at pH > 8.

**Table S1.** Contact Angle and Surface tension values for known liquids.

Fluid Phase	Contact Angle	Surface Tension	$\gamma_L^{LW}$	$\gamma_L^+$	$\gamma_L^-$
Diiodomethane	$50.13 \pm 4.90$	50.8	50.8	0.01	0
Ethylene Glycol	$47.46 \pm 7.87$	48.0	29.0	1.92	47.0
Water	$81.81 \pm 2.74$	72.8	21.8	25.5	25.5

**Table S2.** Surface Energy and Wetting properties modeling of SA-TiO<sub>2</sub>-RGO nanosheets/thin film.

Solid Phase	$\gamma_S^{LW}$	$\gamma_S^+$	$\gamma_S^-$	$\gamma_{sv}$ (mJ/m <sup>2</sup> )	$\Delta G_{131}$ (mJ/m <sup>2</sup> )
SA-RGO-TiO <sub>2</sub>	34.2	0.897	2.619	37.3	-59.09

## References

1. T. N. Lambert, C. A. Chavez, B. Hernandez-Sanchez, P. Lu, N. S. Bell, A. Ambrosini, T. Friedman, T. J. Boyle, D. R. Wheeler and D. L. Huber, *Journal of Physical Chemistry C*, 2009, **113**, 19812-19823.
2. T. N. Lambert, C. C. Luhrs, C. A. Chavez, S. Wakeland, M. T. Brumbach and T. M. Alam, *Carbon*, 2010, doi: 10.1016/j.carbon.2010.1007.1015.
3. R.G. Good, C.J. van Oss, in Modern Approaches to Wettability: Theory and Applications, M.E. Schrader, G. Loeb, Eds. Plenum Press, New York, 1991. pp. 1-27.
4. R.G. Good, M.K. Chaudhury, and C.J. van Oss, in Fundamentals of Adhesion, L.H. Lee, Ed., Plenum Press, New York, 1991. pp. 153-172.